ADVANCED FUNCTIONAL MATERIALS
www.afm-journal.de

Solvent-Induced Octahedral Self-Assembly of Prussian Blue and Its Applications in Sodium-Ion Capacitors

Seunghye Jang, Carsten Korte, Sangmin Lee, and Changshin Jo**

Controlling the morphology and exposed facets of nano/microparticles is crucial for enhancing material properties in electrochemical reactions, photoreactions, and biosensors. However, Prussian Blue (PB), a type of metal–organic framework (MOF), rapidly and stably forms a cubic structure, making shape control difficult and leaving its formation process unclear. Here, the octahedral formation of PB particles in glycerol is discovered, which differs from the cubic particles formed in water. Glycerol slows down the crystallization-growth process of PB, allowing direct observation of a stepwise growth in which cubic seeds initially form and subsequently self-assemble into octahedra. Molecular dynamics (MD) simulation suggests that glycerol molecules stabilize the (111) surfaces of PB crystals over the (100) planes, inducing the self-assembly of PB particles into an octahedral shape. It is also observed that the water-to-glycerol ratio influences PB's surface charge and affects the assembly behavior of PB crystals, resulting in the formation of isolated nanocubes (edge length ≈200 nm), microcubes (edge length ≈1 µm), and octahedra (edge length ≈1 µm). As an active material for sodium-ion capacitors, octahedron-shaped PB, with its significantly higher surface area, exhibits outstanding cycling performance, surpassing cubic PB.

1. Introduction

Prussian Blue (PB) is an attractive metal–organic framework (MOF) used in various applications, including the adsorption of radioactive elements,[1,2] drug delivery platforms,[3] catalysis,[4,5] and as a cathode material in sodium-ion[6,7] and seawater batteries.[8] Controlling the morphology of PB is essential for improving its performance in these fields. For example, Zhang et al. synthesized cubic nanoframe PB with excellent performance in sodium-ion batteries through preferential etching,[9] and Lu et al. proposed a cube-stacked structure for biosensing applications.[10] In addition, several studies have reported the synthesis of unique core–shell structured PBAs to enhance OER activity or other electrochemical properties by maximizing the exposure of active interfaces and modulating electron transfer dynamics.[11,12] However, including these studies, research to date has primarily focused on the transformation of structure[13] derived from cubic frameworks, limiting the ability to induce new morphologies. In a typical synthesis, the final morphology of nano- or microparticles is determined by exposed lattice planes that minimize overall surface energy,[14,15,16] but research on controlling the surface energy of PB is still insufficient.

In addition to controlling the surface energy of particles, understanding the mechanisms of particle nucleation and growth[17,18] is essential for engineering a diverse range of final morphologies.[19,20] Previous studies on PB synthesis have only presented the final morphology of the particles without providing clear insight into the driving forces behind shape formation. This lack of understanding of particle growth stems from the rapid co-precipitation of PB particles when two independent metal-ion-containing solutions are mixed in an aqueous environment. This instantaneous formation of particles makes direct observation of their growth process challenging[21,22] (Figure S1, Supporting Information).

In this study, we present a simple method for controlling the surface energy of PB and propose a fundamental approach to gain deeper insight into its growth behavior by inducing slow particle growth. The slowed particle growth rate, induced by glycerol, enabled direct observation of intermediate stages under a scanning electron microscope (SEM). We observed that PB nanocubes with edge lengths of 100–300 nm first form, followed by their assembly into final octahedral microparticles (**Figure 1**). During solution-phase synthesis, solvent molecules interact with PB, altering its surface properties and controlling growth, as confirmed by molecular dynamics (MD) simulations. We also found that the assembly behavior of PB nanocubes varied

S. Jang, C. Jo
Department of Battery Engineering
Pohang University of Science and Technology (POSTECH)
77 Cheongam-Ro, Nam-Gu, Pohang, Gyeongbuk 37673, Republic of Korea
E-mail: jochangshin@postech.ac.kr
C. Korte
Institute of Energy Technologies
Electrochemical Process Engineering (IET-4)
Forschungszentrum Jülich GmbH
52428 Jülich, Germany
S. Lee, C. Jo
Department of Chemical Engineering
Pohang University of Science and Technology (POSTECH)
77 Cheongam-Ro, Nam-Gu, Pohang, Gyeongbuk 37673, Republic of Korea
E-mail: sminlee@postech.ac.kr
The ORCID identification number(s) for the author(s) of this article can be found under https://doi.org/10.1002/adfm.202508095

DOI: 10.1002/adfm.202508095

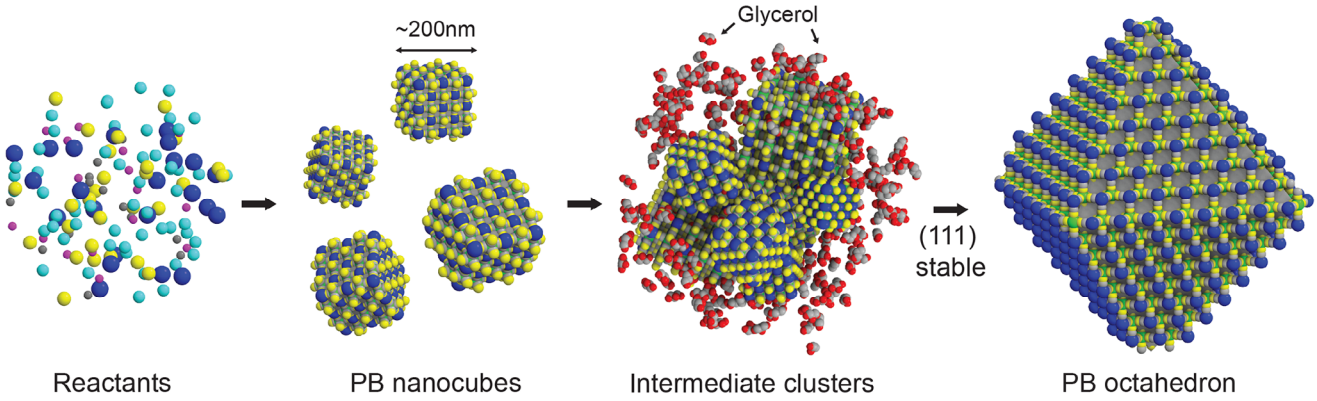

Figure 1. Schematic illustration of PB particle growth in glycerol: The reactant $Na_4Fe(CN)_6$ undergoes decomposition and crystallization to form PB nanocubes, and subsequently, glycerol drives the self-assembly of octahedral-shaped PB to expose the (111) facet.

with solvent conditions (water in glycerol). In the absence of water (0 vol%), nanoparticles assembled into octahedral structures, whereas with increasing water content (2.5–7.5 vol%), they remained as individual cubic nanoparticles, and at 7.5–15 vol%, they further assembled into micrometer-sized cubic structures with slow assembly rates (Figure S2, Supporting Information). A unique observation was that at low water content (2.5–7.5 vol%), nanoparticles remained as individual entities even after 24 h without assembling, and MD simulations prove that this behavior arises from a water-rich inner layer that forms around the particles.

Octahedral-shaped PB, formed through the assembly of nanocubes, offers a significantly larger active surface area compared to cubic PB synthesized via conventional methods. Therefore, it could be a promising candidate as an electrode material for supercapacitors. Using an octahedral-shaped PB-based electrode, we conducted a galvanostatic charge/discharge test in a symmetric cell configuration, and the results confirmed that the octahedral-shaped PB electrode exhibited highly reversible and stable cycling performance compared with conventional cubic PB electrodes. These findings suggest that assembled octahedral-shaped PB can serve as an electrode material for both the anode and cathode in sodium-ion capacitors. Furthermore, solvent-mediated synthesis methods can be applied to regulate PB morphologies, expanding their applicability across various fields.

2. Results and Discussion

2.1. Stepwise Growth of Octahedral-Shaped PB Microparticles in Glycerol

The synthesis of PB in non-aqueous solvents often encounters challenges due to the poor solubility of reaction precursors, necessitating techniques such as solvothermal synthesis in the presence of water[23] or microwave-assisted synthesis[24] to induce reactions. However, glycerol, a highly polar solvent with three hydroxyl groups, effectively dissolves the reactant ($Na_4Fe(CN)_6$) without requiring additional external forces, needing only heating above 50 °C. This enables a significantly simpler process and a mild synthesis environment, allowing for straightforward synthesis. Furthermore, due to its high viscosity, glycerol slows down particle diffusion,[25] which suggests a substantial delay in particle growth due to reduced interparticle interactions.[26] Based on this, we hypothesized that in glycerol, the particle formation and growth process occurs distinctly in separate stages, allowing each step to be individually captured—an aspect previously unobservable due to the rapid synthesis rate in aqueous environments.

To test this hypothesis, PB particles were synthesized in glycerol (Method), and powder samples were collected at different reaction times (2, 6, and 12 h) to examine their morphological evolution via SEM (**Figure 2**). As shown in Figure 2a, after 2 h of reaction, anhydrous $Na_4Fe(CN)_6$, used as a single precursor, supplied both Fe^{3+} and $Fe(CN)_6^{4-}$ ions, resulting in the formation of nano-sized cubic PB particles, which exhibited a tendency to adhere together (Figure 2a,d). This suggests that nucleation and early-stage growth occurred simultaneously in the viscous glycerol environment. After 6 h, no independent cubic nanoparticles remained; instead, all had aggregated into octahedral secondary particles (Figure 2b,e). The clustered particles observed on the surfaces of the secondary particles remained relatively small, ranging from ≈10 to 40 nm. It is speculated that the cubic particles continued to interact in the solvent, undergoing dissolution and reassembly to form larger octahedral secondary particles. This stage is interpreted as a solvent-assisted restructuring driven by surface energy minimization. After 12 h, the final clusters underwent surface ripening to minimize surface energy, resulting in smooth-surfaced, micro-sized octahedral PB particles (Figure 2c,f). This ripening likely involved localized dissolution of high-energy surface facets followed by redeposition onto low-energy facets, ultimately leading to micro-sized PB particles with clean octahedral morphology. By capturing particle images at intermediate reaction stages, we gained a clear understanding of the PB particle growth process in glycerol.

SEM images of cracked particles and TEM analysis of intermediate particles reveal a clear distinction between the surface-assembled nanoparticles and the smaller, irregular nanoparticles filling the interior more compactly (Figure S5a–c, Supporting Information). The inner morphology implies dynamic restructuring, which is likely to occur during the process of exposing specific crystal planes.

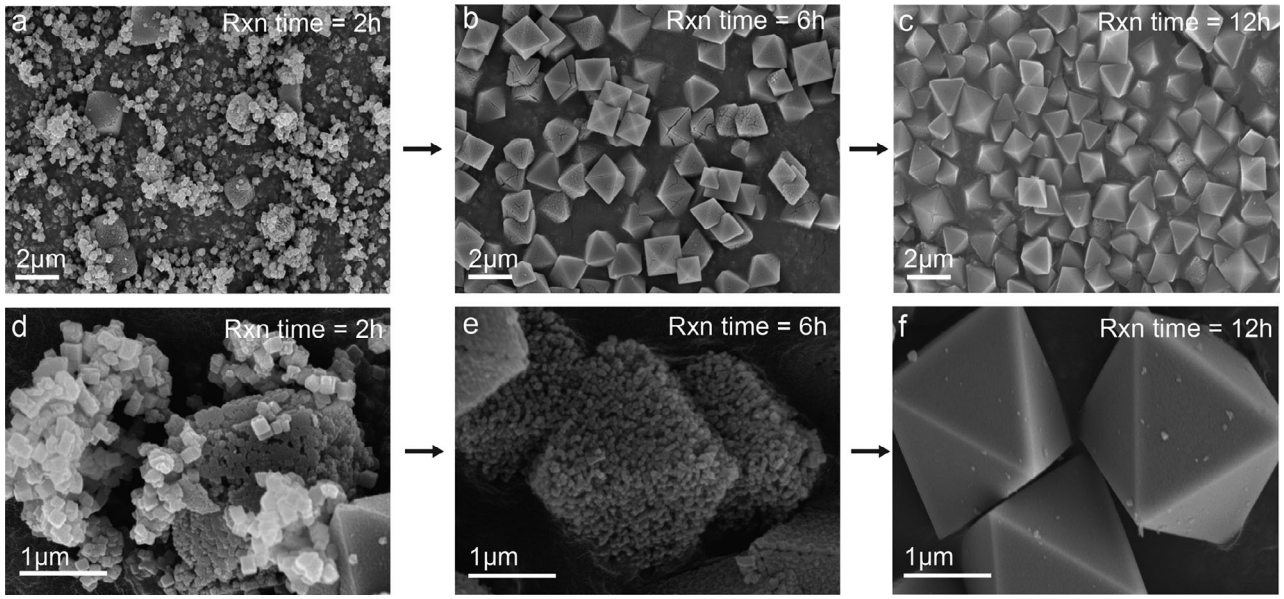

Figure 2. Scanning Electron Microscope (SEM) Image for PB in glycerol according to the reaction time. Reacted for a) 2 h. b) 6 h. c) 12 h, d–f) Zoomed-in views of samples from (a), (b), and (c), respectively.

After 12 h, most PB particles exhibited a smooth, ripened octahedral morphology, though some rare instances of surface-cracked particles were also observed (Figure S6a, Supporting Information). This led to the expectation that prolonged reaction times would result in extended exposure to the solvent, causing stress and eventual structural collapse. To verify this, SEM, TEM, and nano-CT imaging were performed on samples synthesized for 24 h, confirming this phenomenon (Figure S6b,d,f, Supporting Information). Notably, for the first time in PB research, we observed the self-assembly of PB into octahedral structures—a process that had not been reported previously. Beyond simply inducing octahedral formation, our ex situ observations at different synthesis time points provided critical insights into the formation mechanism of PB.

To investigate crystallographic changes during the nucleation and growth of PB particles, X-ray diffraction (XRD) and selected-area electron diffraction (SAED) analyses were conducted. Initially, in the sample reacted for 2 h, most nano-sized PB particles remained independent, though occasional instances of aggregation into octahedral structures were observed. XRD results confirmed that these nano-PB particles exhibited well-defined crystallinity (**Figure 3**a). Subsequently, as the reaction progressed, repeated dissolution and reassembly of particles occurred due to continuous solvent exposure. This led to a decrease in particle size and the formation of randomly oriented aggregates, resulting in broader XRD peaks (Figure 3b). As observed in the SAED pattern at the upper right of Figure 3, the initially crystalline nano-PB particles exhibited a distinct dot pattern, which became elongated during the assembly process.

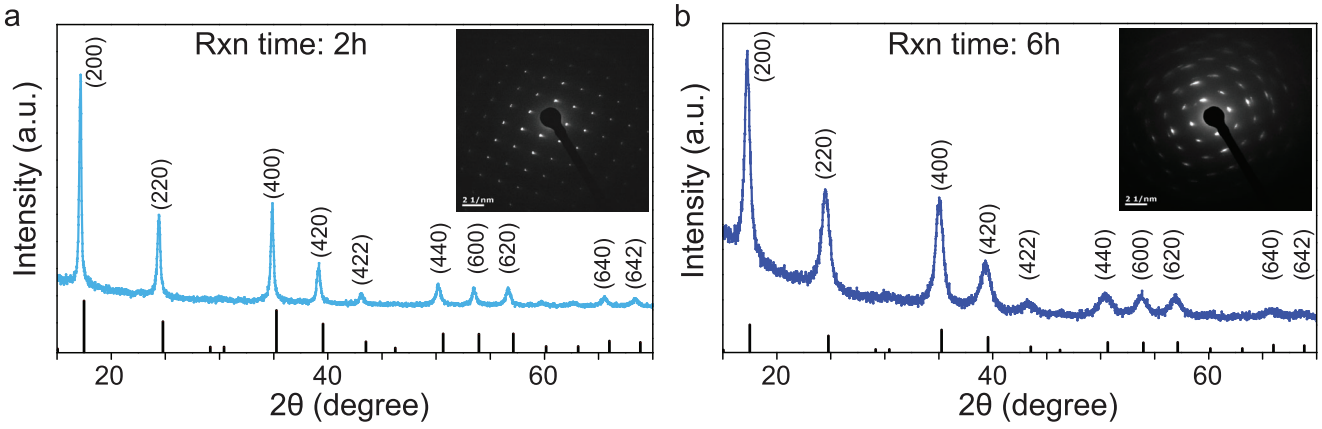

Figure 3. Particle crystallinity analysis. X-ray Diffraction (XRD) for PB, a) before assembly (2 h). b) after assembly (6 h). The bar below XRD peaks represents the JCPDS of PB (#JCPDS 00-001-0239). Selected Area Electron Diffraction (SAED) for PB before and after assembly is located at the upper right corner of each XRD data.

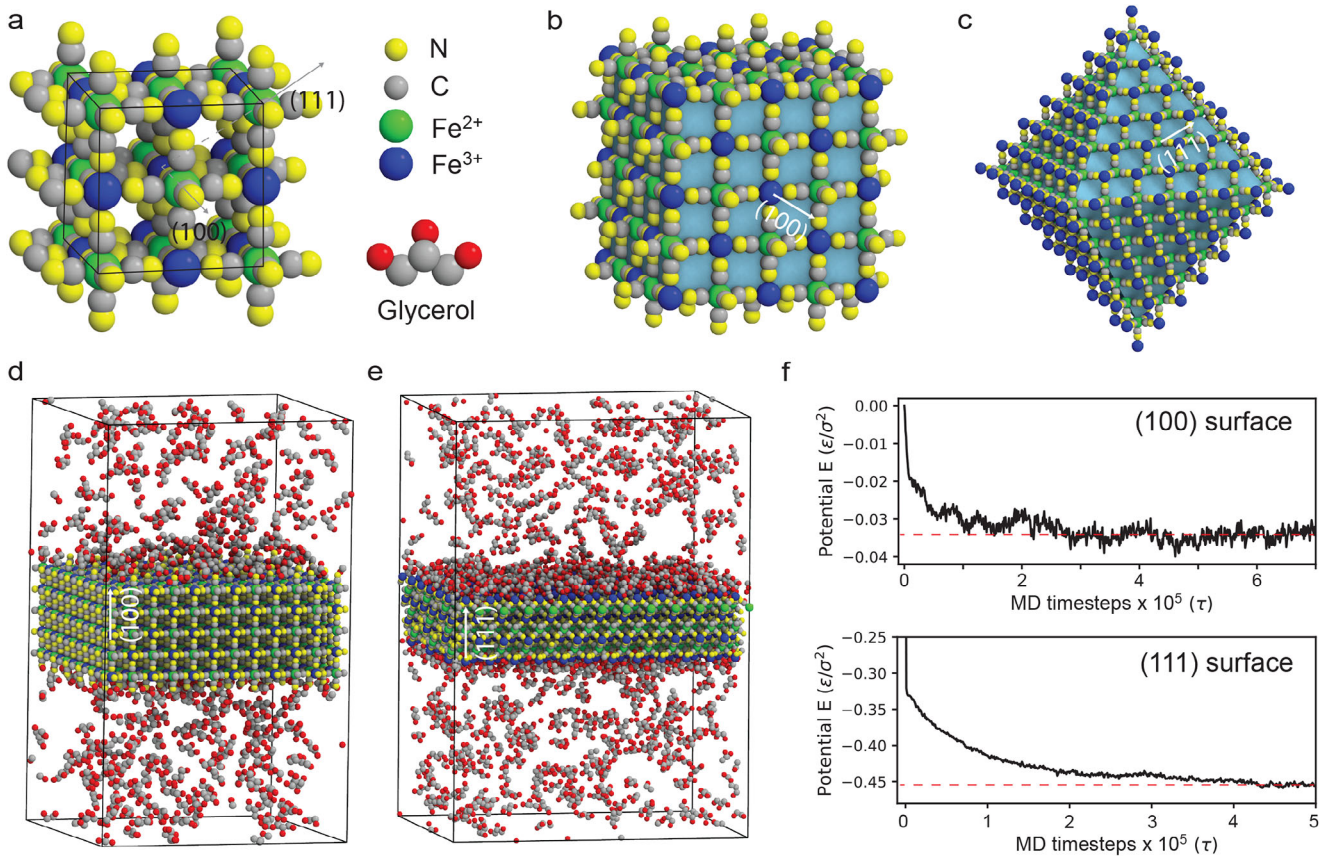

Figure 4. MD simulations for the surface energy calculation in glycerol. a) Unit cell of the PB model structure and CG model of a glycerol solvent. b,c) Atomic configurations of PB particles with a cube (exposing (100) surface) and an octahedron (exposing (111) surface) shape. d,e) MD simulation snapshot for (100) and (111) surface energy calculations. f) Time evolution of potential energy per unit area (/2) for (100) surface (top) and (111) surface (bottom).

2.2. Surface Energy Calculation

The polyhedral shape of particles largely depends on the energy difference of crystal facets.[27] The PB crystal has a cubic lattice structure, and the equilibrium shape of the PB particles synthesized in aqueous solution is a cube exposing six (100) facets, indicating that the (100) surface has the lowest surface energy. In glycerol, on the other hand, we observed the formation of octahedron PB particles exposing eight (111) facets, suggesting that the lowest surface energy is altered to (111) facets. Different PB facets have different atomic configurations (**Figure** 4a–c), and the lowest surface energy of PB will be determined by the chemical interaction between the facet and the solvent molecules.

To test this hypothesis in silico, a simplified simulation model was built to study the interaction between the glycerol molecules and different PB surfaces, using the HOOMD-Blue MD simulation toolkit.[28] In this model, the PB crystal and the glycerol molecules were represented as a rigid crystal lattice and a rigid body molecule, respectively, where constituent atoms are rigidly linked (Figure 4a, Method). The pairwise interaction between charged atoms was modeled by a shifted Gaussian potential[29] to account for the interaction between the PB atoms on the surface and the solvent molecules. To calculate the surface energy of the PB crystal, we exposed a specific lattice plane toward a fluid of solvent in a simulation box with periodic boundary conditions (Figure 4d,e), and the potential energy was monitored until it reached equilibrium (Figure 4f). We confirmed that the (111) surface is more stable than the (100) surface in glycerol, as the potential energy per unit area of the (111) surface ($-4.5 \times 10^{-1}/2$) is lower than that of the (100) surface ($-3.3 \times 10^{-2}/2$). Given the atomic configurations of the PB surface and the size of the glycerol molecule, the (111) surface provides less steric hindrance for the solvents to interact with the charged irons (Fe^{3+}).

2.3. The Understanding of the Interaction between Solvent and Particles

To better understand the interactions between the solvent and particles, we varied the ratio of water to glycerol and observed the resulting changes in particle morphology under SEM with identical 6 h reaction times (**Figure** 5a–c). Unlike the pure glycerol environment where the PB nanocubes assemble into octahedral microparticles (Figure 2), in the 7.5 vol% water environment, the nanocubes did not assemble into microparticles and remained as independent nanocubes (Figure 5a). The nanoparticles did not aggregate even after a prolonged reaction time of 24 h (Figure S7b, Supporting Information), suggesting that the

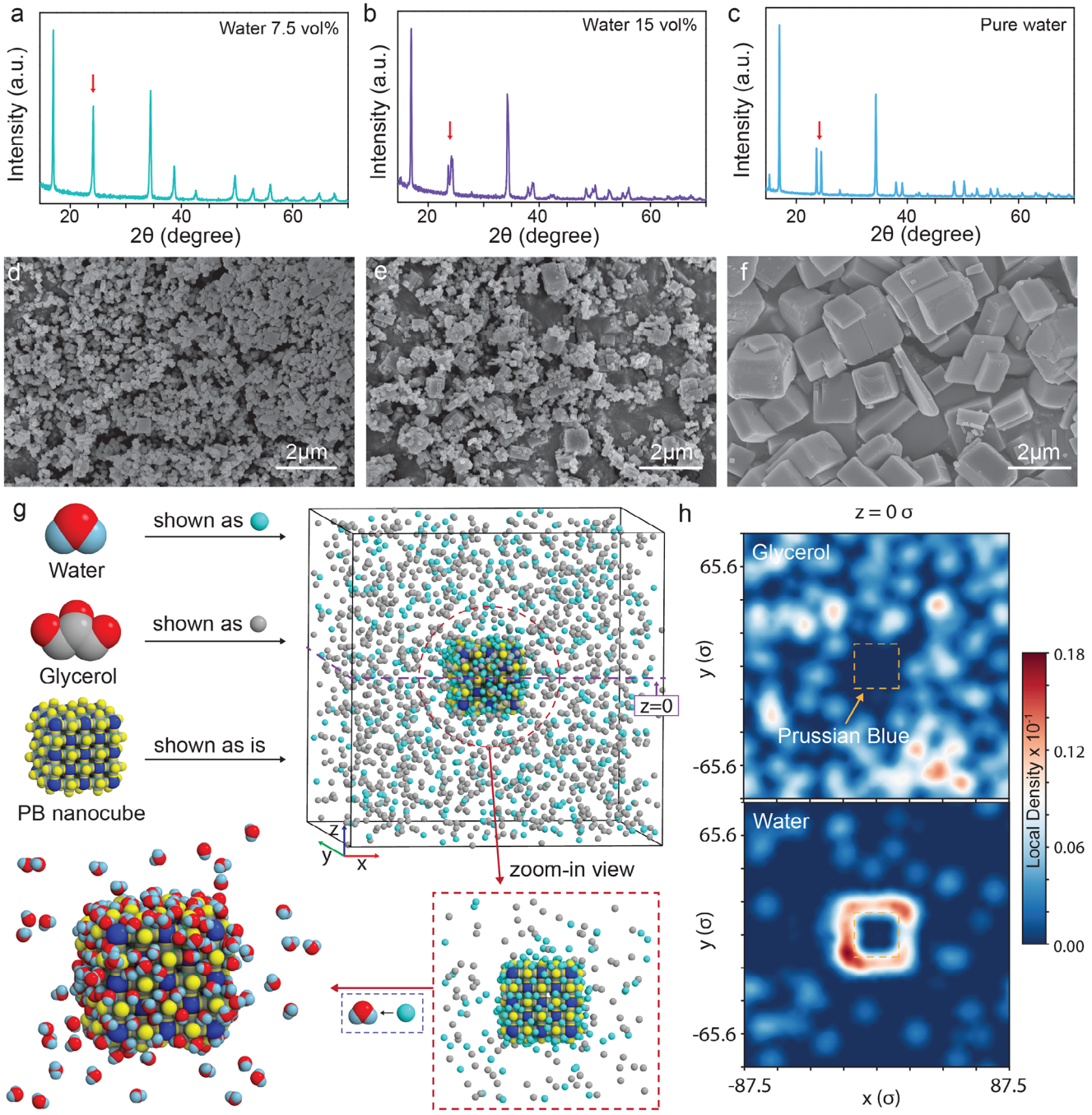

Figure 5. Differences in growth and morphology of PB according to the water-glycerol solvent ratio. XRD and SEM results of a,d) Water: Glycerol = 7.5:92.5, b,e) Water: Glycerol = 15:85, c,f) Water: Glycerol = 100:0 with 6 h reaction time. g) MD simulation result of a PB nanocube in water-glycerol mixed solvent (7.5 vol% of water). (upper left) Explicit solvent model of water and glycerol, and a rigid structure model of PB nanocube. (upper right) An MD simulation snapshot in equilibrium with a simplified solvent representation. (bottom) A zoomed-in view of a PB nanocube. h) Local density analysis of each solvent (top: glycerol, bottom: water) near the PB nanocube.

repulsion between the particles remained balanced. With 15.0 vol% of water, we observed that the nanocubes assembled into cube-shaped microparticles at a very slow rate (Figure 5b). Even after 24 h of reaction, only several microcubes formed, and the aggregated nanometer-sized particles were still largely present (Figure S7d, Supporting Information). In pure water, only microcubes appeared, as expected (Figure 5c).

To understand the delayed growth of PB crystals in the water-glycerol mixture, we conducted MD simulation of a PB nanocube in the 7.5 vol% water environment with explicit solvent models

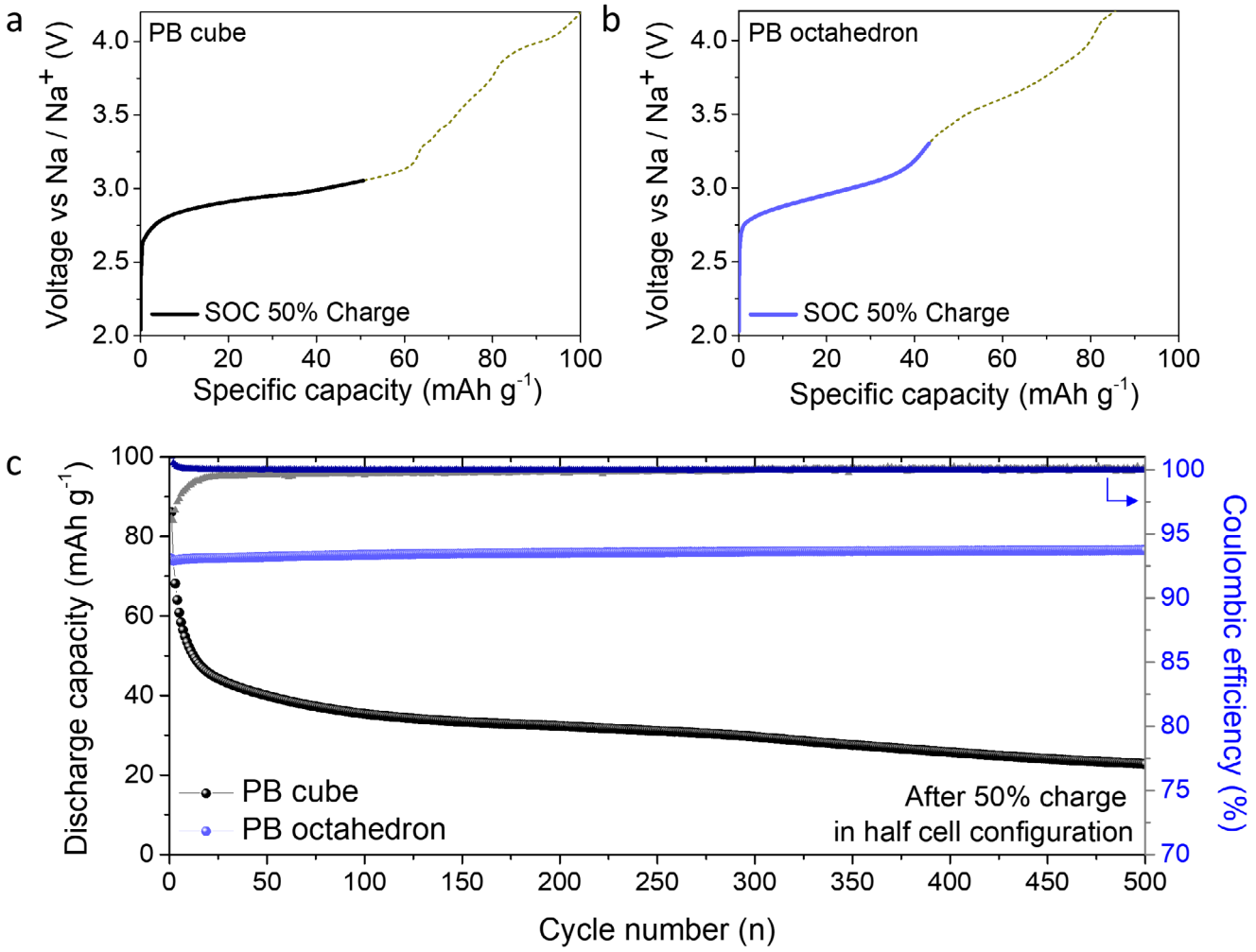

Figure 6. Electrochemical performance evaluation of PB cube and PB octahedron. a,b) Voltage–capacity profile at 50% state of charge of the (a) PB cube, (b) PB octahedron, c) Long-term cycling performance of PB//PB symmetric cells of PB cube and PB octahedron over 500 cycles.

(Figure 5h upper). After equilibration, we confirmed that the concentration of water is notably high in the vicinity of the PB surfaces, while the concentration of glycerol was uniform in the system. We calculated the local density of each solvent (Figure 5h, bottom) and confirmed that a water-rich layer is formed around the PB nanocube. This suggests that sodium ions are more likely to reside within the water-rich layer as the ions have a higher affinity for water than glycerol. This may result in an enhanced electrostatic repulsion between the nanocubes, which consequently prevents or significantly slows down the second–step assembly of the PB nanocubes. In addition, we noted that the presence and insertion of sodium ions into the PB lattice can induce the $Fe^{3+} \rightarrow Fe^{2+}$ transition, which in turn alters the surface chemistry of PB and potentially affects its interaction with solvent molecules. To account for this effect, we constructed an additional MD simulation model in which the interaction between surface iron atoms and solvent molecules (water and glycerol) was weakened (Figure S8, Supporting Information). Even under these modified conditions, a water-rich layer was still observed around the PB crystal. Experimental observations also indicated that increasing the glycerol content in the glycerol–water mixed solvent led to slower reaction kinetics (Figure S10, Supporting Information). It was visually observed that a decrease in glycerol content led to the rapid formation of opaque particles within a short period of time.

We conducted XRD analysis to further characterize the crystal structure of PBs in different water-glycerol ratios (Figure 5d–f). The crystal structure of sodiumcontaining PB depends on sodium content, where the insertion of more than one sodium ion in a unit cell forms a rhombohedral phase, while the incorporation of one or fewer in a unit cell (i.e., low sodium contents) is characterized as a cubic structure.[30,31] In pure glycerol, XRD peaks corresponding to a cubic phase were observed (Figure 3b), indicating a low sodium content of the PB crystal. However, as the water content increased, a transition toward a sodium-rich rhombohedral phase became evident. In particular, at 15 vol% water, the XRD pattern displayed a splitting of the (220) diffraction peak near 22°, which is indicative of a transition toward a rhombohedral phase (Figure 5e).[31] This suggests that the increased water content facilitates the incorporation of more sodium ions, pushing the crystal structure toward a more sodium-rich rhombohedral form. In the pure water

environment, a fully rhombohedral phase was distinctly observed (Figure 5f).

These results support the conclusion that higher water content in the solvent promotes greater sodium incorporation into the PB structure. This trend provides additional insight into the formation of a sodium-rich inner layer and is consistent with previously reported structural behavior of sodium-containing (rich or poor) PB.

2.4. Electrochemical Performance of Octahedral-Shaped PB for Sodium-Ion Capacitor Applications

PB octahedron (refer to the octahedral-shaped PB) exhibits a significantly higher specific surface area (14m2 g^{-1}) compared to PB cube (3m2 g^{-1}, Figure S11, Supporting Information) according to nitrogen adsorption/desorption-based BET analysis. This can be attributed to the difference in morphology: while PB cube consists of micro-sized particles, PB octahedron retains its nanoscale structure, leading to a substantial increase in surface area. Given that PB is widely utilized as an energy storage material, we applied octahedral PB, which contains sodium ions within its structure and possesses a high surface area per unit volume, as an electrode material in a sodium-ion capacitor requiring rapid charge-discharge capability. To evaluate the intrinsic properties of the material, a symmetric cell was fabricated, and charge-discharge experiments were conducted. The PB electrode was prepared as a freestanding electrode with a composition ratio of PB: carbon nanotube (CNT) = 9:1 (wt.%) and a loading density of 10 mg cm^{-2} (Figures S12 and S13, Supporting Information). To assess the practical applicability of the electrode design, we investigated a high-mass-loading electrode (10 mg cm^{-2}), which significantly exceeds typical reported loadings. Despite the increased areal mass, the high-loading electrode exhibited comparable resistance to that of a low-loading (3 mg cm^{-2}) electrode, indicating minimal ionic diffusion limitations under practical conditions (Figure S15, Supporting Information).

To enable a more reliable and fair comparison between PB cube and PB octahedron, half-cells were first assembled using sodium metal as both reference and counter electrodes. Each electrode was charged to 50% of its total charge capacity to ensure an equivalent state of charge (SoC) prior to the construction of symmetric cells (**Figure 6**a,b). This approach allowed for a controlled environment in which sodium ions could participate reversibly in redox reactions under comparable conditions. Notably, PB cube inherently contains a larger amount of sodium within their structure, which may result in a portion of the sodium ions being electrochemically inactive in the symmetric cell configuration, a structural limitation that was considered in the experimental design. Under these standardized conditions, electrochemical cycling at a high rate of 10C revealed that the PB cube suffered a rapid capacity decay, retaining only 33.4% of its initial capacity after 500 cycles. In contrast, the PB octahedron maintained a stable capacity of 75–76 mAh g^{-1} throughout 500 cycles, demonstrating significantly superior high-rate cyclability (Figure 6c). With maintaining the original sodium content within the structure, the cycling test conducted with the same sodium content showed that PB octahedron exhibited superior cycling performance, even at low loading (Figures S14 and S15, Supporting Information).

The PB octahedron exhibits superior capacity retention at high current densities, likely due to its increased surface area and improved ionic and electronic transport pathways. Although its initial sodium content is relatively lower, resulting in slightly reduced capacity at low rates, rate performances and cycle stability under practical conditions are significantly improved. In contrast, cubic PB displays higher overpotentials and suppressed Fe^{2+}/Fe^{3+} redox activity, which can be attributed to lattice water causing active site blockage and undesirable side reactions[32,33] (Figure S16, Supporting Information). Furthermore, EIS data after 500 cycles show that the PB cube exhibits a diminished semicircle and a loss of diffusion-related features, indicating pronounced electrochemical degradation (Figure S17, Supporting Information). Meanwhile, the PB octahedron retains similar impedance characteristics, suggesting stable ion transport and structural integrity. These findings imply that the enhanced electrochemical behavior of octahedral PB results from a synergistic combination of structural advantages and favorable chemical properties. Therefore, we demonstrated that the octahedron-assembled PB can be considered a promising electrode material for both the cathode and anode of sodium-ion capacitors.

3. Conclusion and Outlook

Our strategy for synthesizing PB particles using glycerol significantly expanded our understanding of the growth mechanism and the final morphology of PB particles. Unlike conventional aqueous solvents, high-viscosity glycerol enabled observation of time-dependent particle formation. Nano-cubes formed initially, then gradually assembled into octahedra through solvent-induced dissolution and etching. Octahedral-shaped PB, created through this assembly, exhibits a very large surface area, which demonstrates reversible and stable cycling behavior when applied as an electrode material for capacitors, showing its suitability as both cathode and anode. Our findings are not necessarily limited to glycerol but can be extended to other organic solvents with different chemical properties; for example, an organic solvent that stabilizes (110) surfaces of PB will form a rhombic dodecahedron. This study, which controls solvent interaction and reaction rates to directly observe and understand the synthesis process, offers new insights into the synthesis of materials with diverse shapes and sizes, providing significant potential for advancing material design.

Supporting Information

Supporting Information is available from the Wiley Online Library or from the author.

Acknowledgements

This work was supported by Korea Institute for Advancement of Technology (KIAT) grant funded by the Korea Government (MOTIE) (RS-2024-00419413, HRD Program for Industrial Innovation), Korea Institute of Energy Technology Evaluation and Planning (KETEP) grant funded by the Korea government (MOTIE) (20228510070100), and the National Research Foundation of Korea (NRF) grant funded by the Korea government (MSIT) (No. RS-2024-00411809).

Conflict of Interest

The authors declare no conflict of interest.

Author Contributions

Conceptualization was done by S.J., Methodology was developed by S.J., Investigation was conducted by S.J., S.L., and C.K., Supervision was provided by S.L. and C.J., Writing—original draft was prepared by S.J. and S.L., and Writing—review and editing was carried out by S.J., C.K., S.L., and C.J.

Data Availability Statement

The data that support the findings of this study are available in the supplementary material of this article.

Keywords

dynamic monitoring, facet engineering, morphology control, prussian Blue, self-assembly

Received: March 31, 2025
Revised: June 9, 2025
Published online: July 24, 2025

[1] S. Feng, J. Gao, X. Li, S. Fang, H. Fang, J. Ni, S. Feng, *Sci. Total Environ.* **2024**, *912*, 169365.
[2] J. E. Jung, D. H. Kyoung, S. M. Kang, *Korean Chem. Eng. Res.* **2024**, *62*, 181.
[3] Z. Li, Y. Hu, T. Jiang, K. A. Howard, Y. Li, X. Fan, M. Yu, *Part. Part. Syst. Charact.* **2016**, *33*, 53.
[4] Z. Y. Yu, Y. Duan, J. D. Liu, Y. Chen, X. K. Liu, W. Liu, S. H. Yu, *Nat. Commun.* **2019**, *10*, 2799.
[5] H. Zhang, Q. Jiang, J. H. Hadden, F. Xie, D. J. Riley, *Adv. Funct. Mater.* **2021**, *31*, 2008989.
[6] G. Oh, J. Kim, S. Kansara, H. Kang, H. G. Jung, Y. K. Sun, J. Y. Hwang, *J. Energy Chem.* **2024**, *93*, 627.
[7] X. Liu, Y. Cao, J. Sun, *Adv. Energy Mater.* **2022**, *12*, 2202532.
[8] H. Jeong, S. H. Ahn, C. Jo, *Chem. Eng. J.* **2023**, *465*, 142834.
[9] W. Zhang, Y. Zhao, V. Malgras, Q. Ji, D. Jiang, R. Qi, K. Ariga, Y. Yamauchi, J. Liu, J.-S. Jiang, M. Hu, *Angew. Chem., Int. Ed.* **2016**, *55*, 8228.
[10] D. Lu, H. Jiang, W. Gao, S. G. Liu, Q. Zhao, X. Shi, *Adv. Funct. Mater.* **2023**, *33*, 2208897.
[11] S. Wang, W. Huo, H. Feng, X. Zhou, F. Fang, Z. Xie, J. Jiang, *Small* **2022**, *18*, 2203713.
[12] S. Wang, W. Huo, H. Feng, Z. Xie, J. K. Shang, E. V. Formo, J. Jiang, *Adv. Mater.* **2023**, *35*, 2304494.
[13] J. Nai, X. W. Lou, *Adv. Mater.* **2019**, *31*, 1706825.
[14] W. S. Nam, G. Y. Han, *Korean J. Chem. Eng.* **2003**, *20*, 1149.
[15] H. Sim, J. Lee, T. Yu, B. Lim, *Korean J. Chem. Eng.* **2018**, *35*, 257.
[16] M. M. Ferrer, G. S. Fabris, B. V. de Faria, J. B. Martins, M. L. Moreira, J. R. Sambrano, *Heliyon* **2019**, *5*, 02500.
[17] M. H. Modarres, S. Engelke, C. Jo, D. Seveno, M. De Volder, *Nano Lett.* **2018**, *19*, 228.
[18] M. Ban, J. Lee, J. Kim, S. J. Shin, T. Kim, C. Jo, J. Lee, *Small* **2024**, *20*, 2306154.
[19] C. Jo, J. Hwang, W. G. Lim, J. Lim, K. Hur, J. Lee, *Adv. Mater.* **2018**, *30*, 1703829.
[20] J. Hong, C. Jo, *J. Power Sources* **2024**, *594*, 234006.
[21] Q. Wu, G. Wu, L. Wang, W. Hu, H. Wu, *Mater. Sci. Semicond. Process.* **2015**, *30*, 476.
[22] S. Kjeldgaard, I. Dugulan, A. Mamakhel, M. Wagemaker, B. B. Iversen, A. Bentien, *R. Soc. Open Sci.* **2021**, *8*, 201779.
[23] S. Wang, M. Qin, M. Huang, X. Huang, Q. Li, Y. You, *ACS Appl. Energy Mater.* **2022**, *5*, 6927.
[24] W. Geng, Z. Zhang, Z. Yang, H. Tang, G. He, *Chem. Commun.* **2022**, *58*, 4472.
[25] E. Evoy, A. M. Maclean, G. Rovelli, Y. Li, A. P. Tsimpidi, V. A. Karydis, A. K. Bertram, *Atmos. Chem. Phys.* **2019**, *19*, 10073.
[26] J. Perkins, E. Edwards, R. Kleiv, N. Weinberg, *Mol. Phys.* **2011**, *109*, 1901.
[27] Z. L. Wang, *J. Phys. Chem. B* **2000**, *104*, 1153.
[28] J. A. Anderson, J. Glaser, S. C. Glotzer, *Comput. Mater. Sci.* **2020**, *173*, 109363.
[29] S. Wang, S. Lee, J. S. Du, B. E. Partridge, H. F. Cheng, W. Zhou, C. A. Mirkin, *Nat. Mater.* **2022**, *21*, 580.
[30] S. Baumgart, M. Sotoudeh, A. Groß, *Batter. Supercaps.* **2023**, *6*, 202300294.
[31] W. Wang, Y. Gang, Z. Hu, Z. Yan, W. Li, Y. Li, S. X. Dou, *Nat. Commun.* **2020**, *11*, 980.
[32] Z. Wang, K. Nie, M. T. Sougrati, C. Wang, Z. Liu, J. Wang, J. Wang, *Chem. Eng. J.* **2024**, *488*, 151090.
[33] Z. Wang, M. T. Sougrati, Y. He, P. N. Le Pham, W. Xu, A. Iadecola, J. Wang, *Nano Energy* **2023**, *109*, 108256.